NANO · MICRO small
www.small-journal.com

Au@gap@AuAg Nanorod Side-by-Side Assemblies for Ultrasensitive SERS Detection of Mercury and its Transformation

Aimeng Yuan, Xiaoling Wu, Xiu Li, Changlong Hao, Chuanlai Xu, and Hua Kuang**

As one of the most toxic heavy metal elements, mercury ion (Hg^{2+}) and its methylated product, methylmercury (MeHg) can pose a threat to human health and the environment. Herein, a novel Raman biosensor with cascade sensitivity is developed for Hg^{2+} detection through Au@gap@AuAg nanorod side-by-side assemblies. Due to the strong electromagnetic coupling from the assemblies and core–shell structure, the Raman sensor possesses high sensitivity with the limit of detection (LOD) of 0.001 ng mL^{-1}, which is about one order lower than traditional atomic fluorescence spectrometer (AFS) methods. Moreover, the fabricated biosensor is used to measure residual mercury levels in tissues and eggs of hens fed high-mercury diets, and the results show total mercury in collected egg yolks is 20 times higher than whites. Furthermore, the form of mercury in the eggs is also analyzed by high-performance liquid chromatography coupled with AFS, and, unexpectedly, the methylated product MeHg tends to only be found in egg whites. These interesting differences may indicate a new research direction for the toxicity of mercury in living organisms, and the developed ultrasensitive Surface Enhanced Raman Scattering (SERS) method could pave a broad way for the application of biosensors in Hg detection.

1. Introduction

Mercury, mainly occurring in various forms of elemental Hg, inorganic, and organic Hg, plays an essential role in the environment.[1–4] However, because it is a persistently toxic and biodegradable metal ion,[5,6] inappropriate treatment, and excessive exposure to Hg could result in massive accumulation in organisms. This can cause different health problems, such as nervous system, kidney diseases, and so on.[7–11] More importantly, increased bioavailability of Hg associated with excessive exposure leads to elevated levels of methylmercury (MeHg) in the body, which may also have adverse consequences involving extreme fetal abnormalities and neurotoxicity, and thus become a critical environmental issue.[12–15]

Given that mercury possesses the potential to influence the health of diverse populations, development of methods to effectively monitor and control levels of Hg are necessary. Typically, numerous instrumental analysis methods such as atomic fluorescence spectrometry (AFS),[16] cold atomic absorption spectrometry,[17] inductively coupled plasma-mass spectrometry (ICP-MS),[18] and optical emission spectrometry[19] are used for precise quantification of Hg. These methods are all well-established but inevitably have some problems such as long data acquisition time, expensive instrument maintenance costs, and requirement of professional operation. Recently, some nanosensors such with colorimetry,[20] electrochemistry,[21] fluorescence,[22] and surface enhanced raman scattering (SERS)[23–25] have received interest for determination of Hg. In these sensors, SERS-based biosensors are more unique because of their nondestructive identification and distinct signal enhancement.[26–30] However, the limits of detection (LODs) of the previous reports are on the μg ml^{-1} level, and not suitable for the need of Hg detection. Therefore, the more fast and sensitive method to monitor the environmental mercury are badly in demand.

In this work, a novel Raman biosensor based on the Au@gap@AuAg side-by-side nanorod assemblies has been proposed for highly sensitive Hg ions detection, with strong electromagnetic coupling from the side-by-side assembly and core-gap-shell structure. Consequently, the linear response of SERS intensity to the concentration of Hg^{2+} was achieved. Remarkably, the SERS biosensor was used to measure the total mercury levels of tissues usually consumed by people and egg whites and yolks from Rahman Brown laying hens exposed to high Hg. The total mercury levels in egg yolks were about

A. Yuan, Dr. X. Wu, X. Li, Dr. C. Hao, Prof. C. Xu, Prof. H. Kuang
State Key Laboratory of Food Science and Technology
Jiangnan University
Wuxi, Jiangsu 214122, P. R. China
E-mail: wuxiaoling@jiangnan.edu.cn; kuangh@jiangnan.edu.cn

A. Yuan, Dr. X. Wu, X. Li, Dr. C. Hao, Prof. C. Xu, Prof. H. Kuang
International Joint Research Laboratory for Biointerface and Biodetection and School of Food Science and Technology
Jiangnan University
Wuxi, Jiangsu 214122, P. R. China

A. Yuan, Dr. X. Wu, X. Li, Dr. C. Hao, Prof. C. Xu, Prof. H. Kuang
Collaborative Innovation center of Food Safety and Quality Control in Jiangsu Province
Jiangnan University
Wuxi, Jiangsu 214122, P. R. China

The ORCID identification number(s) for the author(s) of this article can be found under https://doi.org/10.1002/smll.201901958.

DOI: 10.1002/smll.201901958

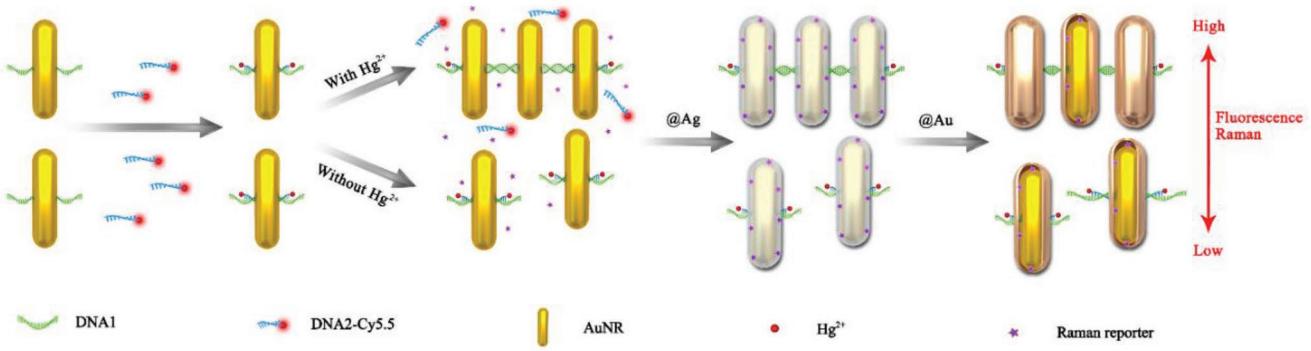

Scheme 1. A Schematic illustration of Au@gap@AuAg nanorod side-by-side assemblies for biosensing Hg ions.

20 times higher than in egg whites, while MeHg tend to only exist in egg whites. This may be because more Hg bound with the higher amount of protein or amino acid in the yolks than that of whites, and higher amount of mercapto amino acid or proteins and methylase enzyme content in the egg whites, which help more inorganic Hg transformed to organic Hg.

2. Results and Discussion

2.1. Illustration of the Au@gap@AuAg Nanorod Side-by-Side Assembly Biosensor

The mechanism of the probe for Hg detection is briefly shown in **Scheme 1**. The developed SERS sensor for Hg^{2+} detection was depended on the T–Hg^{2+}–T coordination chemistry and partly complementary Au NR-DNA (Au NR-DNA1 and DNA1-DNA2-Cy5.5) with deliberately designed A–T mismatches. The PEG-modified Au NRs were conjugated with DNA1 by an Au–S bond and then hybridized with DNA2-Cy5.5 by A–T mismatches, whose fluorescence was likely to be quenched due to close contact with Au NRs. Then, when in presence of Hg target, it guided the transformation of free DNA-decorated Au NRs to form nanorod side-by-side assemblies by the strong T–Hg^{2+}–T interaction, leading to the dissociation of A–T partly complementary and the fluorescence recovery of Cy5.5 dye along with the enhancement of SERS signal. While at the absence of Hg target, the mixture of dispersed AuNR-DNA1-DNA2-Cy5.5 would be stably formed at the room temperature, resulting in the low fluorescence intensity and SERS activity. Thus mercury ions can be detected by the intensity change of fluorescence and SERS. To further amplify the SERS response, the Ag shell coating on the surface of the assemblies and the small nanogap between Au@Ag nanorod assemblies with strong electromagnetic coupling were creatively fabricated. Therefore, the cascade amplified SERS signal could be used for the ultrasensitive detection of mercury, which is reported for the first time.

2.2. Construction of the Au Nanorod Side-by-Side Assemblies

The two methods of transmission electron microscopy (TEM) and ultraviolet–visible (UV–vis) spectra were used to characterize the morphology of the prepared materials. As shown in Figures S1 and S2 (Supporting Information), the synthesized Au NRs, with an aspect ratio of ≈3.1 and UV absorption at the wavelengths of 520 and 718 nm, exhibited good uniformity and dispersity. During the self-assembly process with Hg^{2+} ranging from 0.01 to 10 ng mL^{-1}, as illustrated in Figure S3 (Supporting Information), the blue shift of UV absorption 720 nm wavelength had taken place, which likely indicated a fattened layer after self-assembly.[31–33] Corresponding TEM images were shown in **Figure 1** and Figure S4 (Supporting Information), and they also displayed the larger assemblies at higher Hg^{2+} concentration, resulting from the more formation of T–Hg^{2+}–T and the more dissociation of A–T partly complementary. In addition, as illustrated in **Figure 2**a, the fluorescence intensity at 720 nm increased due to assembly formation and the corresponding recovery of Cy5.5 fluorescence. The original fluorescence spectrum of Cy5.5 was shown as Figure S5 (Supporting Information), which eventually remained stable at 5 ng mL^{-1}. Accordingly, the intensity of the 720 nm peak was chosen to establish a linear relationship with Hg ion concentrations (Figure 2b) and the standard curve of the fluorescence biosensor was calculated as Table S2 (Supporting Information). Similarly, as demonstrated in Figure 2c, with the increasing Hg ions, the larger assemblies provided more sites for Raman tags-4-NTP. This original Raman spectra of 4-NTP was exhibited as Figure S6 (Supporting Information), showing ν(CS), ν(NO_2), and ν(CC) at the band of 1080, 1341, and 1573 cm^{-1}, respectively,[34,35] and the peak at 1341 cm^{-1} was the obviously characteristic SERS peak of 4-NTP which had been chosen for the Hg quantification. Figure 2d and Table S2 (Supporting Information) displayed the standard curve between Raman intensity at 1341.4 cm^{-1} and Hg concentration. It is noted that the limit of detection (LOD) for Hg was 0.008 and 0.007 ng mL^{-1}, based on fluorescence and Raman biosensors, respectively, which is more sensitive than most reported technologies (see Table S3 in the Supporting Information).

2.3. Construction of the Au@gap@AuAg Nanorod Side-by-Side Assemblies

To further advance Hg detection methods, more sensitive and diverse sensors should always be under development. Taking

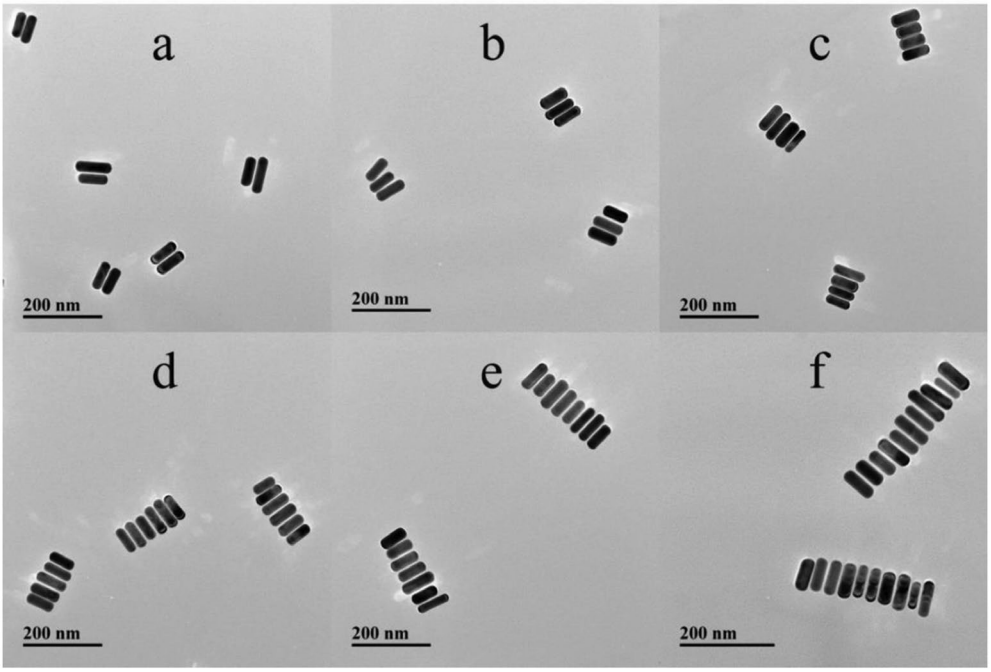

Figure 1. The TEM images of side-by-side oriented gold nanorod assemblies with different Hg^{2+} concentrations: a) 0.01 ng mL^{-1}, b) 0.05 ng mL^{-1}, c) 0.1 ng mL^{-1}, d) 0.5 ng mL^{-1}, e) 1 ng mL^{-1}, f) 5 ng mL^{-1}.

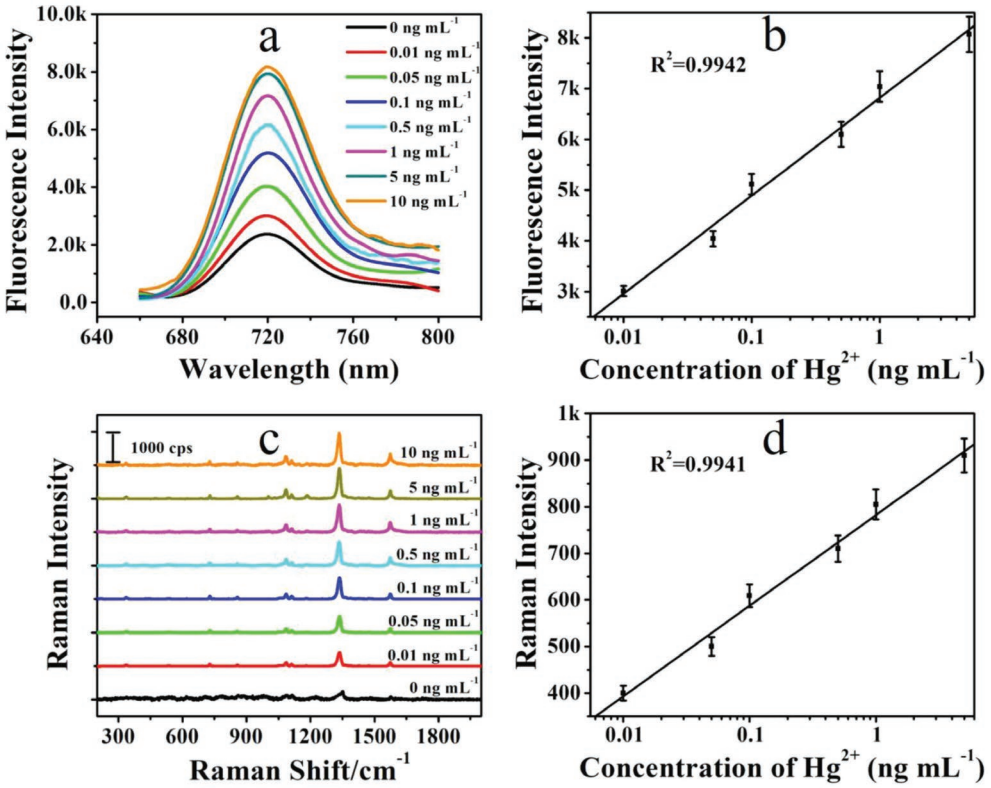

Figure 2. Detection of Hg^{2+} by FL and SERS based on the side-by-side assembly of gold nanorods: a) Fluorescence spectra of the oriented assemblies of gold nanorods at different Hg^{2+} concentrations. b) The linear relationship between the concentration of Hg^{2+} and the corresponding fluorescence intensity. c) Raman spectra from various Hg^{2+} concentrations. d) The standard curve of SERS peak intensities at 1341.4 cm^{-1} over the various Hg^{2+} concentrations.

into account the two main effects on enhancing the Raman signal: electric field and charge-transfer processes,[36,37] Au nanorod side-by-side assemblies were coated with Ag and Au aimed at triggering active electron transformation to increase SERS intensity[38] (see the Supporting Information). To clarify the mechanism of the high sensitivity of the nanoprobes, the electromagnetic simulations were carried out. As the electromagnetic simulations (Figure S7, Supporting Information) shown, the electric field calculated for Au NRs dimer, Au NRs@silver dimer, and the Au NRs@gap@Au shell dimer were 9.8, 19.9, and 50.3 V m^{-1} respectively. The electric field enhancement against the origin Au NRs dimer was calculated to be 1:2.03:5.13. The theoretical results further demonstrated that the ultrastrong electromagnetic enhancement, resulting from the electromagnetic coupling between side-by-side assembly and core-gap-shell structure of the Au@gap@AuAg nanorod assemblies, enabled the excellent sensitivity of the nanoprobes.

Figures S8 (Supporting Information) displayed the various thicknesses of Ag shell with different $AgNO_3$ concentrations, and at Figure S9 (Supporting Information), the absorbance of Ag at 405 nm became much stronger with the thicker Ag shell. And the elemental analysis of the Au@Ag NRs by EDS mapping was carried out as Figure S10 (Supporting Information), from the representative EDS mapping images, Ag shell and Au core were clearly observed, solidly proving the existence of the Ag shell. Under the condition, the successful forming of Au@Ag NR assemblies with Hg^{2+} concentrations from 0.005 to 5 ng mL^{-1} were illustrated as Figures S11 and S12 in the Supporting Information. The results of the Au@Ag NR assembly biosensor method as Figures S13 and S14 (Supporting Information) exhibited, showed that LOD for Hg was 0.003 ng mL^{-1}, which was twice as high as the LOD of the method using the Au NR assembly.

Given that a smaller gap could also improve the signal,[39] Au@gap@AuAg was ultimately constructed after the optimization of gap size. As shown in Figure S15 (Supporting Information), the UV–vis spectra exhibited two characteristic bands with an increasing concentration of $HAuCl_4$ and $AgNO_3$: one at ≈720 nm, and the other near 400 nm. During the process, the peak at 720 nm was most likely from the AuNR core as it became weaker, whereas the other near 400 nm was possibly from the AgAu shell because it became stronger. A shown in Figure S16 (Supporting Information), HRTEM and TEM images were taken of different Au@gap@AuAg nanorod assemblies at 0.01 ng mL^{-1} of Hg, and some different small gaps (0.4, 0.8, 1.2, and 2.0 nm) between core and shell can be observed. The bigger gaps occurred with the increasing concentrations of $HAuCl_4$ and $AgNO_3$ along with the stronger Raman intensity caused by 4-NTP attached to the AgAu shell (Figure S17, Supporting Information). Finally, the Raman intensity reached the highest value using 10 µL of 16 mM $AgNO_3$ and 30 µL of 0.125 mM $HAuCl_4$ as Figure S18 (Supporting Information) displays, and the gap of ≈1.2 nm was finally chosen.

Then, the Au@Ag NR assemblies were coated with Au under the optimized conditions. As shown in Figure S19 (Supporting Information), the dominant UV–vis absorption of Au@gap@AuAg NR assemblies near 720 and 400 nm both appeared, and **Figure 3** showed the successful assembly of Au@gap@AuAg NRs superstructures. **Figure 4**a represents the corresponding Raman intensities of different Hg concentrations, and the system of Au@gap@AuAg NR assemblies had stronger intensities than the Au@Ag and Au NRs assemblies at the same Hg level. Overall, the Raman intensity significantly increased in relation to not only the Au/Ag/Au substrate platform to which the signal tags attached but also the gap space in which the 4-NTPs existed. Meanwhile, the calibration plot, Figure 4b,

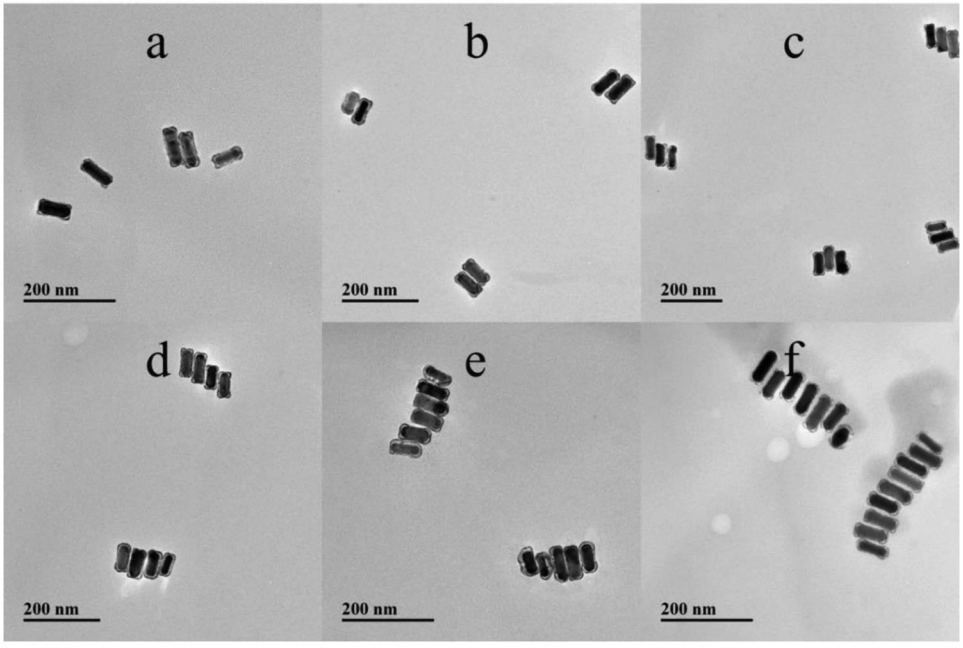

Figure 3. The TEM images of Au@gap@AuAg nanorod assemblies over various Hg^{2+} concentrations: a) 0.005 ng mL^{-1}, b) 0.01 ng mL^{-1}, c) 0.05 ng mL^{-1}, d) 0.1 ng mL^{-1}, e) 0.5 ng mL^{-1}, f) 1 ng mL^{-1}.

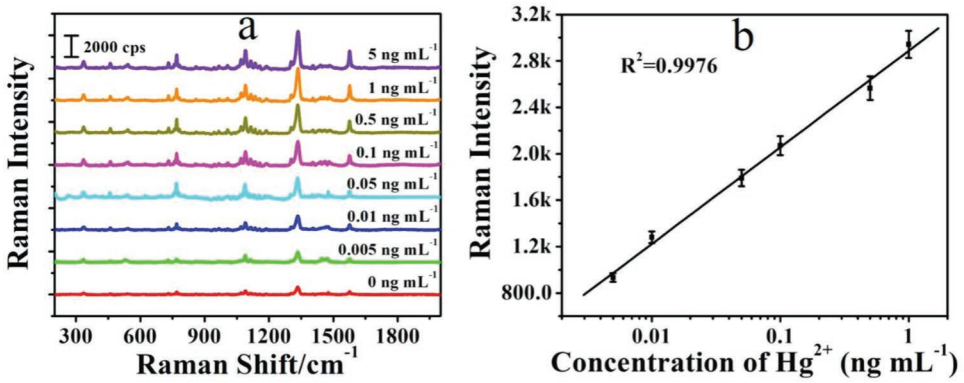

Figure 4. Detection of Hg^{2+} by SERS based on the side-by-side assembly of Au@gap@AuAg nanorods: a) Raman spectra collected from different Au@gap@AuAg nanorod side-by-side assemblies at various Hg^{2+} concentrations. b) The standard curve of SERS peak intensities at 1341.4 cm^{-1} over the different Hg^{2+} concentrations.

shows a good linear relationship between the peak intensities and target concentrations in the range of 0.005–1 ng mL^{-1} with a detection limit of 0.001 ng mL^{-1}. In all, the LOD of Au@gap@AuAg assemblies biosensor is seven times lower than that based on the AuNR assemblies. Moreover, their LOD is three times lower than that of Au@Ag assemblies.

The monodispersity of the proposed biosensor was explored by the dynamic light scattering of different nanoprobes (Figure S20, Supporting Information). As shown in DLS data, there were no larger aggregations for the Au@gap@AuAg NRs as well as other controls NPs. In addition, to study the stability and reproducibility of the biosensor, the sensor was carried out at different times (1, 2, 4, 8, 12 h) (Figure S21, Supporting Information), and five parallel working sensor were prepared for detecting Hg ions (Figure S22, Supporting Information). The change in SERS intensity at 1341 cm^{-1} remained 96.32% of its original intensity, which indicated the good stability of the biosensor and the relative standard deviation (RSD) of the measurement for the five sensors was 3.82%, which showed the biosensor possessed good reproducibility.

And in order to evaluate the selectivity of the proposed biosensor, ten interfering chemicals were selected to be tested. This reveals that interfering chemicals even in much higher concentrations had almost no influence on the sensor as shown in Figure S23 (Supporting Information), which further demonstrated the high specificity of the developed method for the Hg^{2+} detection. Hence, the developed SERS biosensor showed a lower detection limit with excellent selectivity for Hg detection and would likely to have prospective applications in detecting Hg ions.

2.4. Application in Assessing Total Hg Levels in Chicken Tissues and Eggs

To evaluate the accuracy and practical application in real samples, the designed Raman biosensor was utilized to assess total Hg levels in chicken tissues and eggs. As **Figure 5**a shows, the content of mercury varied greatly among different tissues for $HgSO_4$-fed chickens. The highest total mercury levels of all tissues were clearly found in the liver, in accordance with previous studies[40] due to glutathione, cysteine, and other chemical substances containing sulfhydryl. Besides, the mercury contents of the $HgSO_4$-fed eggs (egg whites and egg yolks) were also monitored by our developed method. Higher mercury content was observed in egg yolks than in egg whites. Interestingly, the 10 d laid egg yolks and whites with significantly higher levels than 5, 15, and 20 d (Figure 5b,c), indicated that laid eggs could help chickens lower mercury burden in their body, which bioaccumulated at successive dietary exposure. And the total mercury levels in egg yolks were about 20 times higher than that of in egg whites, this may be because more Hg bound with the higher amount of protein or amino acid in the yolks than that of whites. These results were all confirmed by the traditional method (AFS), with a good agreement with that of AFS (Figure 5d), indicating that the presented way was suitable for the determination of Hg in biological samples.

2.5. Analysis of MeHg in Eggs by HPLC-AFS

Considering the observed significant differences in total mercury levels between egg whites and yolks, the chemical forms of mercury were analyzed by HPLC-AFS. It was found that there was nearly no methylmercury in egg whites and yolks for control group (Figures S24 and S25, Supporting Information), while higher levels of methylmercury (retention time of 3.297 min) were found in egg whites than that in yolks for experimental group (Figures S26 and S27, Supporting Information). This may result from higher amount of mercapto amino acid or proteins and methylase enzyme content in the egg whites, which help more inorganic Hg transformed to organic Hg. Besides, the 10 d laid egg yolks had significantly higher methylmercury levels (0.017 mg kg^{-1}) than 5, 15, and 20 d (Figure S28, Supporting Information), which was consistent with total mercury trends.[41] To briefly summarize, mercury was removed from chickens' bodies through deposition in the egg yolks, but the methylated form accumulated mainly in the whites.

In all, a novel Raman biosensor with excellent sensitivity for detecting Hg ions has been successfully developed, which will not be eliminated in the laboratory sample analysis

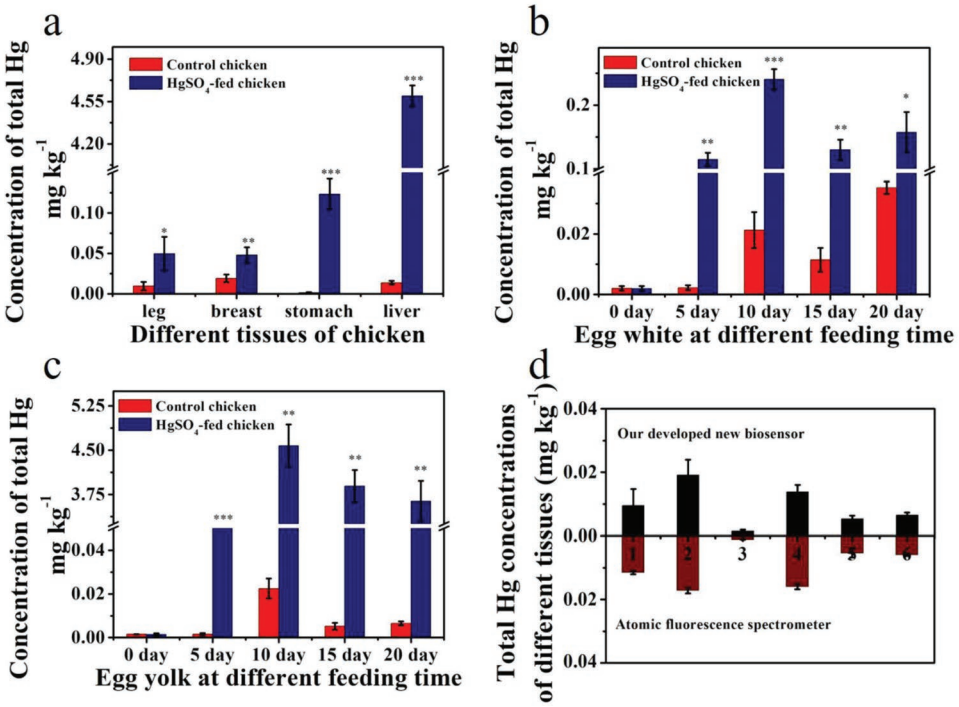

Figure 5. Detection of total Hg in chickens. a) The mercury levels in different tissues after 20 d of control-fed (diets without $HgSO_4$) and $HgSO_4$-fed chickens as determined by our new method with concentrations in mg per kg dried mass. b) The mercury levels in egg whites at different times for control and $HgSO_4$-fed chickens. c) The mercury levels in egg yolks at different times for control and $HgSO_4$-fed chickens. d) Comparing the detection of mercury in tissues from control chickens at day 20 by AFS and our new sensor: (1) leg, (2) breast, (3) stomach, (4) liver, (5) egg white, (6) egg yolk. *P*-values according to analysis of *t*-test: $*p < 0.05$, $**p < 0.01$, $***p < 0.001$.

and can be used to measure the total Hg levels in cultured chickens. These results were also confirmed by AFS. In addition, HPLC-AFS was utilized to assess the methylmercury levels in eggs from cultured chickens. These results may provide some inspiration for mercury detection and toxicity research.

3. Experimental Section

Construction of the Hg Biosensor Based on Au@gap@AuAg Nanorod Side-by-Side Assemblies: Au nanorods (Au NRs) were synthesized as mentioned in the Supporting Information.[42,43] Then, 100 µL purified Au NRs were modified with 4 µL single-stranded T-rich DNA1 (100 µM) for 8 h and next connected by 4 µL A-rich DNA2-Cy5.5 (100 µM) for 8 h (see Table S1 in the Supporting Information). In the presence of Hg ions, Au NR assemblies would be formed by the T–Hg^{2+}–T mispairing interaction.[44,45] The Raman and fluorescence spectra of the assemblies were measured in the solution. Moreover, 10 µL $AgNO_3$ (4 mM) and 5 µL ascorbic acid (50 mM) were used to form the Ag shell, followed by adding Raman reporter 4-NTP with a final concentration 10 µM. The resulting Au@gap@AuAg was obtained by adding 30 µL $HAuCl_4$ (0.125 mM). The different assemblies corresponding with the Raman spectra of various Hg concentrations were able to be detected.

Measurement of Hg and MeHg in Cultured Chicken Tissues and Eggs: Sample preparation for Hg detection based on the Raman biosensor was conducted by wet digestion.[46,47] Approximately 0.1 g dry weight of tissues and eggs was separately put in 50 mL centrifuge tubes, which was followed by adding 5 mL of 65% HNO_3. Then, the solution was heated to 120 °C on a graphite furnace digestion instrument for 30 min before 2 mL of H_2O_2 was added. Thirty minutes later, a pure liquid was obtained. The digestion solution was analyzed by the established Raman biosensor and the results were validated by AFS. Furthermore, an AMW/UV combined reactor with an AFS detection system was used for reversed-phase chromatography (RPC) experiments to detect MeHg.[48,49]

Cultured Chicken Tissues and Eggs Samples: In the current study, 50 Rahman Brown laying hens were divided into two groups, one was fed with 15 mg Hg^{2+} per kg feed (22 mg kg^{-1} $HgSO_4$) and the normal feed without the additional $HgSO_4$ was used as the controlled group. A total number of 50 egg samples (five samples per group) were collected, both yolks and whites were separately analyzed according the culture time. In addition, 12 samples of the tissues and organs (six replicates from each group) were also obtained.

Supporting Information

Supporting Information is available from the Wiley Online Library or from the author.

Acknowledgements

This work was financially supported by National Key R&D Program (2017YFC1600306). All animal studies in this work were performed according to institutional ethical guidelines and were approved by the Committee on Animal Welfare of Jiangnan University.

Conflict of Interest

The authors declare no conflict of interest.

Keywords

Au@gap@AuAg nanorods, mercury, side-by-side assemblies, transformation, ultrasensitive SERS detection

Received: April 18, 2019
Revised: May 2, 2019
Published online:

[1] D. P. Krabbenhoft, E. M. Sunderland, *Science* **2013**, *341*, 1457.
[2] P. J. Landrigan, R. Fuller, N. J. R. Acosta, O. Adeyi, R. Arnold, N. Basu, A. B. Balde, R. Bertollini, S. Bose-O'Reilly, J. I. Boufford, P. N. Breysse, T. Chiles, C. Mahidol, A. M. Coll-Seck, M. L. Cropper, J. Fobil, V. Fuster, M. Greenstone, A. Haines, D. Hanrahan, D. Hunter, M. Khare, A. Krupnick, B. Lanphear, B. Lohani, K. Martin, K. V. Mathiasen, M. A. McTeer, C. J. L. Murray, J. D. Ndahimananjara, F. Perera, J. Potocnik, A. S. Preker, J. Ramesh, J. Rockstrom, C. Salinas, L. D. Samson, K. Sandilya, P. D. Sly, K. R. Smith, A. Steiner, R. B. Stewart, W. A. Suk, O. C. P. van Schayck, G. N. Yadama, K. Yumkella, M. Zhong, *Lancet* **2018**, *391*, 462.
[3] Y. Chen, Y. G. Yin, J. B. Shi, G. L. Liu, L. Hu, J. F. Liu, Y. Cai, G. B. Jiang, *Crit. Rev. Environ. Sci. Technol.* **2017**, *47*, 2415.
[4] H. Gonzalez-Raymat, G. Liu, C. Liriano, Y. Li, Y. Yin, J. Shi, G. Jiang, Y. Cai, *Environmen. Pollut.* **2017**, *229*, 69.
[5] X. Li, D. Yin, J. Li, R. Wang, *Arch. Environ. Contam. Toxicol.* **2014**, *67*, 104.
[6] Y. L. Li, B. He, L. G. Hu, X. Huang, Z. J. Yun, R. Z. Liu, Q. F. Zhou, G. B. Jiang, *Talanta* **2018**, *178*, 811.
[7] G. Bjorklund, M. Dadar, J. Mutter, J. Aaseth, *Environ. Res.* **2017**, *159*, 545.
[8] S. W. Tan, J. C. Meiller, K. R. Mahaffey, *Crit. Rev. Toxicol.* **2009**, *39*, 228.
[9] G. Bjorklund, J. Mutter, J. Aaseth, *Arch. Toxicol.* **2017**, *91*, 3787.
[10] J. Aaseth, B. Hilt, G. Bjorklund, *Environ. Res.* **2018**, *164*, 65.
[11] Z. Yu, J. Zhang, D. Yin, *PLoS One* **2016**, *11*, e0154529.
[12] M. R. Karagas, A. L. Choi, E. Oken, M. Horvat, R. Schoeny, E. Kamai, W. Cowell, P. Grandjean, S. Korrick, *Environ. Health Perspect.* **2012**, *120*, 799.
[13] M. J. P. Ropero, N. R. Farinas, R. Mateo, J. J. B. Nevado, R. C. R. Martin-Doimeadios, *Environ. Sci. Pollut. Res.* **2016**, *23*, 6074.
[14] C. Gu, H. Xu, G. Qiu, *Environ. Chem.* **2013**, *32*, 926.
[15] Y. L. Li, B. He, J. J. Gao, Q. S. Liu, R. Z. Liu, G. B. Qu, J. B. Shi, L. G. Hu, G. B. Jiang, *Environ. Pollut.* **2018**, *238*, 213.
[16] D. L. F. da Silva, M. A. P. da Costa, L. O. B. Silva, W. N. L. dos Santos, *Food Chem.* **2019**, *273*, 24.
[17] O. Caylak, S. G. Elci, A. Hol, A. Akdogan, U. Divrikli, L. Elci, *Food Chem.* **2019**, *274*, 487.
[18] R. F. Lepak, R. S. Yin, D. P. Krabbenhoft, J. M. Ogorek, J. F. DeWild, T. M. Holsen, J. P. Hurley, *Environ. Sci. Technol. Lett.* **2015**, *2*, 335.
[19] C. Zheng, L. Hu, X. Hou, B. He, G. Jiang, *Anal. Chem.* **2018**, *90*, 3683.
[20] T. Tolessa, Z.-Q. Tan, Y.-G. Yin, J.-F. Liu, *Talanta* **2018**, *176*, 77.
[21] A. L. Suherman, K. Ngamchuea, E. E. L. Tanner, S. V. Sokolov, J. Holter, N. P. Young, R. G. Compton, *Anal. Chem.* **2017**, *89*, 7166.
[22] J.-Y. Yang, T. Yang, X.-Y. Wang, M.-L. Chen, Y.-L. Yu, J.-H. Wang, *Anal. Chem.* **2018**, *90*, 6945.
[23] Y. Shi, N. Chen, Y. Su, H. Wang, Y. He, *Nanoscale* **2018**, *10*, 4010.
[24] X. Zhang, Z. Dai, S. Si, X. Zhang, W. Wu, H. Deng, F. Wang, X. Xiao, C. Jiang, *Small* **2017**, *13*, 1603347.
[25] Z. Duan, X. Zhang, T. Ye, X. Zhang, S. Dong, J. Liu, X. Xiao, C. Jiang, *ACS Appl. Mater. Interfaces* **2018**, *10*, 25737.
[26] Z. Zhang, L. Wen, L. Jiang, *Chem. Soc. Rev.* **2018**, *47*, 322.
[27] X. Wu, C. Hao, J. Kumar, H. Kuang, N. A. Kotov, L. M. Liz-Marzan, C. Xu, *Chem. Soc. Rev.* **2018**, *47*, 4677.
[28] M. Yilmaz, E. Babur, M. Ozdemir, R. L. Gieseking, Y. Dede, U. Tamer, G. C. Schatz, A. Facchetti, H. Usta, G. Demirel, *Nat. Mater.* **2017**, *16*, 918.
[29] H. Zhang, C. Wang, H.-L. Sun, G. Fu, S. Chen, Y.-J. Zhang, B.-H. Chen, J. R. Anema, Z.-L. Yang, J.-F. Li, Z.-Q. Tian, *Nat. Commun.* **2017**, *8*, 15447.
[30] L.-B. Zhong, Q. Liu, P. Wu, Q.-F. Niu, H. Zhang, Y.-M. Zheng, *Environ. Sci. Technol.* **2018**, *52*, 5812.
[31] B. Sharma, P. Bugga, L. R. Madison, A.-I. Henry, M. G. Blaber, N. G. Greeneltch, N. Chiang, M. Mrksich, G. C. Schatz, R. P. Van Duyne, *J. Am. Chem. Soc.* **2016**, *138*, 13952.
[32] M. Zhang, D. J. Magagnosc, I. Liberal, Y. Yu, H. Yun, H. Yang, Y. Wu, J. Guo, W. Chen, Y. J. Shin, A. Stein, J. M. Kikkawa, N. Engheta, D. S. Gianola, C. B. Murray, C. R. Kagan, *Nat. Nanotechnol.* **2017**, *12*, 228.
[33] W. Ma, H. Kuang, L. Xu, L. Ding, C. Xu, L. Wang, N. A. Kotov, *Nat. Commun.* **2013**, *4*, 2689.
[34] Z. Qian, D. S. Ginger, *J. Am. Chem. Soc.* **2017**, *139*, 5266.
[35] S. Tanwar, K. K. Haldar, T. Sen, *J. Am. Chem. Soc.* **2017**, *139*, 17639.
[36] Z. Y. Bao, W. Zhang, Y. L. Zhang, J. J. He, J. Y. Dai, C. T. Yeung, G. L. Law, D. Y. Lei, *Angew. Chem., Int. Ed.* **2017**, *56*, 1283.
[37] C. L. Hao, L. G. Xu, W. Ma, X. L. Wu, L. B. Wang, H. Kuang, C. L. Xu, *Adv. Funct. Mater.* **2015**, *25*, 5816.
[38] Z. Yin, Y. Wang, C. Song, L. Zheng, N. Ma, X. Liu, S. Li, L. Lin, M. Li, Y. Xu, W. Li, G. Hu, Z. Fang, D. Ma, *J. Am. Chem. Soc.* **2018**, *140*, 864.
[39] L. Xu, S. Zhao, W. Ma, X. Wu, S. Li, H. Kuang, L. Wang, C. Xu, *Adv. Funct. Mater.* **2016**, *26*, 1602.
[40] K. P. Kenow, M. W. Meyer, R. Rossmann, B. R. Gray, M. T. Arts, *Environ. Toxicol. Chem.* **2015**, *34*, 1870.
[41] Y. Chen, X. Cheng, F. Mo, L. Huang, Z. Wu, Y. Wu, L. Xu, F. Fu, *Electrophoresis* **2016**, *37*, 1055.
[42] L. B. Wang, Y. Y. Zhu, L. G. Xu, W. Chen, H. Kuang, L. Q. Liu, A. Agarwal, C. L. Xu, N. A. Kotov, *Angew. Chem., Int. Ed.* **2010**, *49*, 5472.
[43] X. X. Wang, L. G. Xu, C. L. Hao, C. L. Xu, H. Kuang, *Environ. Sci. Technol. Lett.* **2018**, *5*, 500.
[44] Y. Zhu, L. Xu, W. Ma, Z. Xu, H. Kuang, L. Wang, C. Xu, *Chem. Commun.* **2012**, *48*, 11889.
[45] S.-H. Wu, B. Zhang, F.-F. Wang, Z.-Z. Mi, J.-J. Sun, *Biosens. Bioelectron.* **2018**, *104*, 145.
[46] M. Esposito, S. Cavallo, E. Chiaravalle, O. Miedico, R. Pellicano, G. Rosato, P. Sarnelli, L. Baldi, *Environ. Monit. Assess.* **2016**, *188*, 326.
[47] R. F. L. Ribeiro, A. Germano, *Microchem. J.* **2015**, *121*, 237.
[48] D. P. C. de Quadros, B. Campanella, M. Onor, E. Bramanti, D. L. G. Borges, A. D'Ulivo, *Spectrochim. Acta, Part B* **2014**, *101*, 312.
[49] R. Siyuan, S. Kae Jye, Y. Lim Wei, X. Yan, C. Wenlong, *ACS Nano* **2015**, *9*, 11218.